

RESEARCH ARTICLE

Biochemical studies of two lytic polysaccharide monooxygenases from the white-rot fungus *Heterobasidion irregulare* and their roles in lignocellulose degradation

Bing Liu¹, Åke Olson², Miao Wu¹, Anders Broberg¹, Mats Sandgren^{1*}

1 Department of Molecular Sciences, Swedish University of Agricultural Sciences, Uppsala, Sweden,

2 Department of Forest Mycology and Plant Pathology, Swedish University of Agricultural Sciences, Uppsala, Sweden

* mats.sandgren@slu.se



OPEN ACCESS

Citation: Liu B, Olson Å, Wu M, Broberg A, Sandgren M (2017) Biochemical studies of two lytic polysaccharide monooxygenases from the white-rot fungus *Heterobasidion irregulare* and their roles in lignocellulose degradation. PLoS ONE 12(12): e0189479. <https://doi.org/10.1371/journal.pone.0189479>

Editor: Daniel Cullen, USDA Forest Service, UNITED STATES

Received: October 16, 2017

Accepted: November 27, 2017

Published: December 11, 2017

Copyright: © 2017 Liu et al. This is an open access article distributed under the terms of the [Creative Commons Attribution License](https://creativecommons.org/licenses/by/4.0/), which permits unrestricted use, distribution, and reproduction in any medium, provided the original author and source are credited.

Data Availability Statement: All relevant data have been included in the paper.

Funding: This work was financially supported by the Swedish Energy Agency (<http://www.energimyndigheten.se/>) through the grant 40144-1 to M.S. The funders had no role in study design, data collection and analysis, decision to publish, or preparation of the manuscript.

Competing interests: The authors have declared that no competing interests exist.

Abstract

Lytic polysaccharide monooxygenases (LPMO) are important redox enzymes produced by microorganisms for the degradation of recalcitrant natural polysaccharides. *Heterobasidion irregulare* is a white-rot phytopathogenic fungus that causes wood decay in conifers. The genome of this fungus encodes 10 putative Auxiliary Activity family 9 (AA9) LPMOs. We describe the first biochemical characterization of *H. irregulare* LPMOs through heterologous expression of two CBM-containing LPMOs from this fungus (*H*LPMO9H, *H*LPMO9I) in *Pichia pastoris*. The oxidization preferences and substrate specificities of these two enzymes were determined. The two LPMOs were shown to cleave different carbohydrate components of plant cell walls. *H*LPMO9H was active on cellulose and oxidized the substrate at the C1 carbon of the pyranose ring at β -1,4-glycosidic linkages, whereas *H*LPMO9I cleaved cellulose with strict oxidization at the C4 carbon of glucose unit at internal bonds, and also showed activity against glucomannan. We propose that the two LPMOs play different roles in the plant-cell-wall degrading system of *H. irregulare* for degradation of softwood and that the lignocellulose degradation mediated by this white-rot fungus may require collective efforts from multi-types of LPMOs.

Introduction

Fungi play a critical role in decomposing plant biomass in nature [1]. Wood rotting fungi, including brown-rotting and white-rotting species, are known as efficient degraders of lignocellulosic biomass [2]. Woody biomass is mainly composed of primary and secondary plant cell walls, which consist of three major groups of building blocks; cellulose, hemicellulose together with pectin (primary) or lignin (secondary), respectively [3]. As the major constitution found in mature wood, the secondary cell walls have complex three-dimensional structures in which the highly ordered cellulose micro-fibrils are embedded in hemicellulose, and lignin fills the space between and interconnect cellulose and hemicellulose. All three components

together create a recalcitrant structure that protects plant cells from microbial degradation [3]. Brown-rot fungi act predominately on cellulose and hemicellulose, while white-rot fungi have the capability to efficiently degrade both the lignin fraction and the wood polysaccharides [2,3]. The main difference between the cell walls of softwood (e.g. pine and spruce) and hardwood (e.g. birch, aspen and oak) is the chemical composition and structure of the hemicellulose fraction, in which softwood contains mostly glucomannan but hardwood is mostly composed of xylan [3,4].

The basidiomycete white-rot fungus *Heterobasidion annosum* (Fr.) Bref. *sensu lato* is a serious pathogen of conifer trees, which has efficient wood degradation capabilities. The economic losses caused by *H. annosum* s.l are at least 790 million Euros per year for European forest owners due to growth reduction and devaluation of timber at harvest [5]. *H. annosum* s.l causes annosus root rot in conifers in boreal and temperate forests in the northern hemisphere [6] by infecting host trees via exposed fresh wood in wounds or stump surfaces where it grows in and colonizes the wood. *H. annosum* s.l grows through the heartwood into the root system and can spread from one tree to another trees via root-to-root contacts [7]. *H. annosum* s.l is a species complex that consist of of five phylogenetically distingt species with partly overlapping geographic distrubution and host preferences [8–10]. In Europe there are three species present (*H. annosum sensu stricto* (s.s.), *H. parviporum* and *H. abietinum*) and in North American there are two species (*H. irregulare* and *H. occidentale*) [8–10]. *H. irregulare* infects and decays mostly pine trees and junipers and can grow within living trees and dominate the decomposition of wood during the competition with other fungi [5,9].

The genomes of *Heterobasidion* spp. have been shown to encode a large arsenal of putative carbohydrate active enzymes (CAZymes) and oxidative enzymes for degrading plant cell walls [11]. Lytic polysaccharide monooxygenases (LPMOs) are a class of recently described copper-dependent redox enzymes that are found both in fungi and bacteria [12]. It has been proposed that LPMOs catalyze oxidative cleavage of linkages between glycan residues in polysaccharides by employing molecular oxygen and external electron donors [13,14]. Cu(I) is used to activate O₂ to form a Cu(II)-superoxyl or a Cu(II)-oxyl reactive intermediate, and thereafter add a single oxygen either at the C1 or the C4 position of the two adjacent glycan residues at the scissile bond. The redox cycle of active-site Cu is thought to be coupled to the delivery of two electrons by an external electron donor [15]. LPMOs are generally thought to be very important components in the enzyme system of plant cell wall-degrading microorganisms for efficient cellulose degradation [16,17] due to their unique capability to introduce oxidative cleavage on the surface of crystalline cellulose [18,19]. It is generally believed that the introduction of new chain ends in the crystalline micro-fibrils by LPMOs creates new starting points for other processive cellulolytic enzymes like cellobiohydrolases [16,19]. The overall structures of LPMOs share a common β -sandwich architecture with the active site positioned on a flat surface of the molecule. The active site of LPMOs is a conserved copper-bound motif composed of two histidine residues, where one of the histidine residues is the N-terminal of the mature protein after removal of the signal peptides [20].

LPMOs have been categorized into four Auxiliary Activity (AA) families (AA9, AA10, AA11, and AA13) in the classification system of Carbohydrate-Active enZymes (CAZymes, www.cazy.org) [21,22]. Families AA9 and AA10 contain the largest numbers of unique proteins. AA9 contains only fungal LPMOs, while bacterial LPMOs are mainly found in AA10. Most of the hitherto characterized AA9 LPMOs show catalytic activity against cellulose and some of them are also active on various hemicellulosic substrates, whereas AA10 LPMOs have been found to be mostly active on chitin but some of them are also on hemicellulose [21,22]. Currently only a few LPMOs belonging to AA11 and AA13 have been identified [21,22]. These two AA families differ from AA9 and AA10 through their unique structural features or

substrate specificity. AA11 LPMOs share some common structural features with both AA9 and AA10, and AA13 LPMOs are found to have activities against starch.

Genes encoding AA9 LPMOs have been identified in a wide range of different fungi, including ascomycetes and basidiomycetes, with an average number of AA9 genes at 7.4 and 8.0 respectively [21]. Among basidiomycetes, white-rot fungi have shown to have a larger number of genes encoding AA9 LPMOs (9–32) than brown-rot fungi (2–10) [21,23]. The best characterized fungal LPMO systems at present are the three ascomycetes *Neurospora crassa* (9 out of 14) [18,24–29], *Podospora anserine* (6 out of 31) [30–32] and *Myceliophthora thermophila* (4 out of 22) [33–35]. The characterization of those three ascomycete systems have shown varied substrate specificities of LPMOs on different types of cellulosic and hemicellulosic substrates, which suggests that individual LPMOs may play different roles in both cellulose and hemicellulose degradation. Characterization of individual LPMOs in a white-rot fungal systems have not been as well addressed as the ascomycete systems so far. The only white-rot fungi with more than one LPMO characterized so far are *Pestalotiopsis* sp. [36] and *Gloeophyllum trabeum* [37,38]. It was shown that the two LPMOs from *Pestalotiopsis* sp. (PsLPMO9A and PsLPMO9B) oxidize insoluble cellulose at different positions, but no information is available in terms of substrate specificity [36]. *G. trabeum* LPMO9A-2 (GtLPMO9A-2) was shown to have oxidative cleaving activities against both cellulose as well as different types of hemicellulosic substrates, including xyloglucan and glucomannan [37]. *G. trabeum* LPMO9B (GtLPMO9B) was shown to act synergistically with an endoglucanase or a xylanase on the saccharification of pretreated woody biomaterials [38], but the enzyme activity of GtLPMO9B alone is not clear. The abundance of AA9-encoding genes in white-rot fungi suggest that white-rot fungi may also have a similar machinery of using multiple types of oxidative enzymes for liberating individual polysaccharide components from the recalcitrant structures of plant cell walls during fungal growth on woody substrates.

The *Heterobasidion irregulare* genome contains 10 putative AA9 genes which have been named HiAA9A through J [39]. Two previous transcriptomics studies have shown that five of putative AA9 genes in *H. irregulare* (HiAA9A, HiAA9B, HiAA9D, HiAA9H, HiAA9I) were considerably up-regulated when the fungus was cultivated on pure cellulose and woody biomaterials, compared to a glucose control [11,39]. HiAA9D, HiAA9H and HiAA9I are predicted to have a C-terminal carbohydrate binding module family 1 (CBM1) linked to their AA9 catalytic domains [39]. The CBM1 domains have been demonstrated to be strong cellulose binding modules, and the catalytic domains linked to CBM1 domains are often reported to have strong cellulose binding affinity [40]. The expression patterns of the *H. irregulare* AA9 genes that contain CBM1 (HiAA9D, HiAA9H, HiAA9I) were similar to two cellobiohydrolases (CBH) in *H. irregulare* (HiCel7A and HiCel6A). This suggests that AA9 proteins are co-expressed with the CBHs, and therefore very likely to be involved in cellulose degradation [11]. None of the 10 LPMOs in the *H. irregulare* genome has been characterized to date and their enzyme activities and substrate preferences are unknown.

The aim of this study was to gain insight into the oxidative biomass-degrading enzyme system of the white-rot fungus *H. irregulare* by exploring the enzymatic activities of some CBM-containing LPMOs on a broad range of lignocellulosic substrates, in order to increase our knowledge of the functional diversification of LPMOs in this fungal system. Two LPMOs from *H. irregulare* were heterologously expressed in the methylotrophic yeast *Pichia pastoris*. The regioselectivity and substrate specificity of these two enzymes were characterized and their biochemical properties were compared with previously characterized AA9 LPMOs. The potential contributions of these two enzymes on lignocellulose degradation in the native system of *H. irregulare* are discussed.

Materials and methods

CRISPR/Cas9-mediated LPMO expression in *P. pastoris*

Preparation of transformation plasmids. The predicted coding sequences of *HiLP-MO9H* and *HiLP-MO9I* were retrieved from the JGI *H. irregulare* Genome Portal (<http://genome.jgi.doe.gov/Hetan1/Hetan1.home.html>). Both LPMO sequences including the native secretion signal sequences were synthesized *de novo* (GeneArt ThermoFisher, Buckinghamshire, UK). All the assembly fragments were prepared by PCR with the primers designed using NEBuilder Assembly tool (<http://nebuilder.neb.com/>), as shown in Table 1. Transformation vectors were constructed by performing Gibson assembly with corresponding DNA fragments using NEBuilder HiFi DNA Assembly Master Mix (New England Biolabs, USA).

Homologous recombination donor plasmid. Each of the synthesized LPMO sequences was inserted upstream of the pGAP promoter in the pGAPZ α A vector (Invitrogen, San Diego, CA) using PCR and Gibson Assembly with primer pairs “pGAPZ α A_Fw and pGAPZ α A_Rv” in combination with the primer pairs “*HiLP-MO9H*_Fw and *HiLP-MO9H*_Rv” and “*HiLP-MO9I*_Fw and *HiLP-MO9I*_Rv”, respectively. The homologous recombination (HR) donor plasmids were constructed by assembling the following three fragments into pMA vector (Invitrogen, San Diego, CA) by Gibson assembly. Fragment one was amplified from the recombinant pGAPZ α vector by PCR using primer pairs “pGAP_LPMO_Zeo_Fw and pGAP_LPMO_Zeo_Rv”, which contains one expression cassette of one LPMO (*HiLP-MO9H* or *HiLP-MO9I*) with C-terminal 6x Hisditine tag and one following cassette for Zeocin resistance. Fragment two and Fragment three are homologous recombination arms with length of 991 bp to either left or right of the directed cleavage site of Cas9 enzyme, which were cloned from the genome of *Pichia pastoris* X33 strain (Invitrogen, San Diego, CA) by PCR using corresponding primer pairs “Left_HR_Arm_Fw and Left_HR_Arm_Rv” or “Right_HR_Arm_Fw and Right_HR_Arm_Rv”.

Plasmids expressing Cas9 and gRNA. Cas9 expression plasmid and gRNA expression plasmid were built on the basis of the constructs pGAP_HsCas9_DAS1 and pTEV1_StRNA2_AOX1TT respectively that were designed by Weninger [41]. For Cas9 expression plasmid, three fragments were assembled into pMA vector, including pGAP promoter which is amplified from pGAPZ α vector (Invitrogen, San Diego, CA), encoding sequence of human (*Homo sapiens*) codon-optimized Cas9 (*HsCas9*) which is cloned from p414-TEF1p-Cas9--CYC1t plasmid (Addgene plasmid no. 43802, Cambridge, USA) and a synthesized fragment (GeneArt ThermoFisher, Buckinghamshire, UK) containing SV40 signal sequence, DAS1 terminator and PASR yeast replication origin in a sequential order.

The gRNA plasmid was constructed by assembling the synthesized fragment pTEV1_StRNA2_AOX1TT (GeneArt ThermoFisher, Buckinghamshire, UK) containing the target sequence “ACCAGATCCCGGTGTGGGAA” into pMA vector (GeneArt ThermoFisher, Buckinghamshire, UK).

***P. pastoris* transformation.** The preparation of competent *P. pastoris* cells and transformation were performed using previously described methods [41]. The HR donor plasmid was linearized by treatment of FastDigest Sfi I (Fermentas, ThermoFisher, USA) at 50°C for 20 h. 40 μ l of *P. pastoris* X33 competent cells were mixed with 1 μ g linearized HR donor plasmid, 0.5 μ g Cas9 plasmid and 0.5 μ g gRNA expression plasmid. Plasmids were introduced into *P. pastoris* cells by electroporation. Successful transformants expressing *HiLP-MO9H* and *HiLP-MO9I* were obtained after 3 days incubation at 30°C on solid yeast extract peptone dextrose (YPD; 10 g/l yeast extract, 20 g/l peptone, 20 g/l glucose) medium containing 100 μ g/ml Zeocin (Invitrogen, San Diego, CA).

Table 1. Primers for assembly of transformation vectors.

Vector		Sequence 5'→3'
pGAP_LPMO_zeocin plasmid	<i>HiLPMO9H_Fw</i>	TGAACAACACTATTTTCGAAACGATGTTTTTCACAGCCGCTC
	<i>HiLPMO9H_Rv</i>	CTGAGATGAGTTTTTGTCTCAAGCACTGTGAGTAATATGC
	<i>HiLPMO9I_Fw</i>	TGAACAACACTATTTTCGAAACGATGTTGTTCAGTCTTCTC
	<i>HiLPMO9I_Rv</i>	CTGAGATGAGTTTTTGTCTTAGGCACCTGGCTATAGTAG
HR donor plasmid	pGAP_LPMO_Zeo_Fw	GCATTCTTTCCTTCTTTTTGTAGAAATGTCTTGGTG
	pGAP_LPMO_Zeo_Rv	CAGATCCCGGTGTGGGCAAATTAAGCCTTCGAG
	Left HR arm_Fw	CGAATTGGCGGAAGGCCGTCAAGGCCGATGTCCAAGAAGTCGTCATC
	Left HR arm_Rv	ACATTTCTACAAAAGAAGGAAGAATGCAATCGAG
	Right HR arm_Fw	AAGGCTTTAATTTGCCACACCCGGATCTGGTC
	Right HR arm_Rv	GGCAGTGAGCGGAAGGCCCATGAGGCCAGCTATATGAAGAGTTTATGGAGGAGCATTG
Cas9 plasmid	pGAP_promoter_Fw	CGAATTGGCGGAAGGCCGTCAAGGCCGATTTTTGTAGAAATGTCTTGGTG
	pGAP_promoter_Rv	GTACTTCTTGTCCATCGTTTCGAAATAGTTGTTC AATTG
	HsCas9_Fw	AACTATTTTCGAAACGATGGACAAGAAGTACTCCATTG
	HsCas9_Rv	TCTTTTCTTCTTTGGGTCTCCACCGAGCTGAGA
	SV40_DAS1TT_PARS_Fw	CAGCTCGGTGGAGACCCAAAGAAGAAAAGAAAGTTAAAC
	SV40_DAS1TT_PARS_Rv	GGCAGTGAGCGGAAGGCCCATGAGGCCAGTCGACAATTAATATTACTTATTTTGG
GPD gRNA plasmid	pTEV1_SiRNA2_AOX1TT_Fw	CGAATTGGCGGAAGGCCGTCAAGGCCGATTCGAGATAAGCTGGGGGAAC
	pTEV1_SiRNA2_AOX1TT_Rv	GGCAGTGAGCGGAAGGCCCATGAGGCCAGGCACAAACGAAGGTCTCAC
pGAPZαA backbone	pGAPZαA_Fw	GAACAAAACTCATCTCAGAAG
	pGAPZαA_Rv	CGTTTCGAAATAGTTGTTC AATTG
pMA backbone	pMA_Fw	CTGGGCCTCATGGGCCTT
	pMA_Rv	ATGCGGCCTTGACGGCCTTC

<https://doi.org/10.1371/journal.pone.0189479.t001>

Heterologous protein expression. *P. pastoris* were pre-cultured in 25 ml YPD medium (25 µg/ml OF WHAT) for 20 h in a shaking incubator at 30°C, 130 rpm. 5 ml pre-culture was transferred to 1L YPD medium in a 3L-baffled flask and cultivated for 24 h at 28°C with 110 rpm orbital shaking. *P. pastoris* cells were removed by centrifugation at 5000 × g for 30 min at 25°C, and the culture supernatant was first filtered through a 0.45-µm PES membrane filter, and thereafter through a 0.2-µm PES membrane.

Protein purification and preparation

Filtered culture supernatants containing either *HiLPMO9H* or *HiLPMO9I* were adjusted with ammonium sulfate ((NH₄)₂SO₄) to 1 M and 1.5 M respectively in 20 mM TRIS buffer pH 7.5. The samples were applied onto a two inter-connected 5 ml HiTrap Phenyl FF HS columns (GE Healthcare Biosciences, Uppsala, Sweden), followed by a step elution with 20 mM TRIS buffer pH 7.5. The eluate was desalted using a 500 ml BioGel P-6DG column (Bio-Rad Laboratories, Richmond, USA) pre-equilibrated in 20 mM TRIS buffer pH 7.5. The retained desalted sample was purified using 5 ml Ni²⁺-charged HiTrap chelating HP column (GE Healthcare Biosciences, Uppsala, Sweden) with a step elution of 20 mM TRIS buffer pH 7.5 containing

200 mM imidazole. After buffer exchange into 20 mM BisTRIS buffer pH 6.5, the *HiLPMO9H* sample was purified using 4.7 ml HiScreen CaptoQ ImpRes column (GE Healthcare Biosciences, Uppsala, Sweden) with a gradient from 0 to 250 mM sodium chloride (NaCl) in 50 ml of 20 mM BisTRIS buffer, pH 6.5. The *HiLPMO9I* sample in 20 mM TRIS buffer pH 7.5 containing 1.5 M $(\text{NH}_4)_2\text{SO}_4$ was applied onto 4.7 ml HiScreen Phenyl HP column (GE Healthcare Biosciences, Uppsala, Sweden), followed by a reverse gradient from 1.5 M to 0 M ammonium sulfate in 25 ml of 20 mM TRIS buffer pH 8.0. The fractions containing the target protein with the right molecular size, as estimated by SDS-PAGE analysis, were pooled and concentrated to 1 ml using a Vivaspın 20 concentration tube with a 10 kDa cutoff by centrifugation at $5,000 \times g$ for 20 minutes. A size-exclusion chromatography step was applied as the final polishing step for both LPMOs using a 120 ml Superdex 75 column (GE Healthcare Biosciences, Uppsala, Sweden), and using 20 mM sodium acetate (NaOAc) buffer, pH 5.5 containing 150 mM NaCl, as running buffer. After Cu(II) saturation by incubation with 1 mM CuSO_4 at 25°C for 1 hour, the purified protein samples were buffer exchanged into 10 mM NaOAc pH 5.5 by using pre-equilibrated SpinTrap G-25 column (GE Healthcare Biosciences, Uppsala, Sweden) with 2-min centrifugation at $800 \times g$.

Protein purity was assessed by SDS-PAGE electrophoresis on TGX Stain-Free Precast Gels with Precision Plus Protein Unstained Protein Standards (Bio-Rad Laboratories, Richmond, USA). The calculation of protein concentration was based on absorbance at 280 nm measured on a Nanodrop spectrophotometer, theoretical molecular weights and molar absorption coefficients (*HiLPMO9H*: 1.62; *HiLPMO9I*: 1.37) computed using ProtParam tool on ExPASy server (<http://web.expasy.org/protparam/>). The N-glycosylation and O-glycosylation sites of the expressed proteins were predicted on NetNglyc server (<http://www.cbs.dtu.dk/services/NetNGlyc/>) and NetOGlyc server (<http://www.cbs.dtu.dk/services/NetOGlyc/>), respectively. The deglycosylation trials were performed using α -mannosidase from *Canavalia ensiformis* (Sigma-Aldrich, Germany) with a ratio of 1:40 (w/w) to the purified LPMO samples, and incubation at 30°C overnight, and the effects on molecular size was monitored by SDS-PAGE analysis.

Biochemical characterization of *HiLPMO9H* and *HiLPMO9I*

Enzyme activity assays. Enzyme activity reactions were performed in 200- μl mixtures containing 1 μM enzyme (*HiLPMO9H* or *HiLPMO9I*), in 1 mM ascorbic acid (Asc.) and each of the following substrates: 10 mg/ml reduced phosphoric acid swollen cellulose (PASC), 0.4 mg/ml cellohexose, 2 mg/ml carboxymethyl cellulose (CMC), 2 mg/ml xyloglucan, 2 mg/ml glucomannan, 2 mg/ml barely glucan, 2 mg/ml galactomannan and 2 mg/ml glucuronoxylan, in 5 mM NaAc buffer pH 6.0 in 2 ml round-bottom microcentrifugic tubes. The substrates were mixed with one of the enzymes or equivalent volume of milliQ water (as control), and freshly prepared ascorbic acid was added as the last step prior to incubation. The PASC activity reactions were incubated in a thermomixer (Eppendorf, Hamburg, Germany) at 50°C for 16 h with 1000 rpm shaking. The incubation of reaction with the other substrates was performed at 30°C for 16 h with shaking at 600 rpm for samples with polysaccharide substrates and without shaking for samples with cello-oligosaccharides. Control reactions were performed in the same conditions in absence of enzyme. Reactions were stopped by boiling the reaction samples at 95°C for 5 min. The reaction samples were thereafter centrifuged at $13,300 \times g$ for 5 min. The supernatant was isolated and used to examine the generation of oxidized product. To simplify the analysis of the product profile in the following analysis, samples from reaction with glucomannan were subjected to treatment with an Endoglucanase (*MtEG7*) from *Myceliophthora thermophila*, which was kindly provided by the research group of Prof. Paul

Christakopoulos at Luleå University of Technology, Sweden. The treatment was performed by 1-h incubation at 37°C with 1 µM MtEG7 in 100 µl of sample supernatant.

PASC was prepared following the protocol by Wood *et al* [42]. PASC in reduced form were prepared following the method described by Westereng *et al* [43]. Cellohexose (G6), xyloglucan from tamarind seed, konjac glucomannan (low viscosity), barely β-1,3-1,4-glucan (medium viscosity) and locus 1-4-β-D-Mannan were purchased from Megazyme (Bray, Ireland). carboxymethyl cellulose (CMC) and birchwood xylan were obtained from Sigma-Aldrich (Germany).

Product analysis of enzyme reaction. The supernatants of enzyme reactions were subjected to a series of -product analysis by high performance anion-exchange chromatography with pulsed amperometric detection (HPAEC-PAD), matrix-assisted laser desorption/ionization time-of-flight mass spectrometry (MALDI-TOF MS) and electrospray ionization mass spectrometry (ESI-MS/MS) as described as below.

HPAEC was performed using a CarboPac PA1 2×250 mm analytical column (Dionex Corp., Sunnyvale, CA) with eluent A (0.1 M NaOH) and B (0.1 M NaOH + 1M NaOAc) using an ICS3000 system equipped with a pulsed amperometric detector (Dionex Corp., Sunnyvale, CA). The system was run at a constant flow rate of 0.25 ml/min at 30°C for all the sample analysis in the study. Samples from the reactions with cellulosic substrates (PASC, CMC, G6) and samples after endoglucanase treatment were analyzed using the elution gradient described by Isaksen *et al* [27]. Sample analyses from reactions with hemicellulosic substrates was following the 75-min stepwise elution method described by Agger *et al* [28].

MALDI-TOF analysis were performed following the protocol established by Vaaje-Kolstad *et al* [13]. Samples of 1 µl were mixed with 2 µl of 9 mg/ml 2,5-dihydroxybenzoic acid (DHB) in 30% acetonitrile on a MTP 384 steel target plate (Bruker Daltonics, Bremen, Germany). After dried under nitrogen flow, samples were analyzed using ULtraFlex II MALDI-TOF Mass spectrometer (Bruker Daltonics, Bremen, Germany) and data were acquired in positive-ion reflection mode.

ESI-MS/MS analysis was carried out on a Bruker maXis Impact mass spectrometer (ESI-Q-TOFMS) (Bruker Daltonics, Bremen, Germany) operated in positive mode scanning *m/z* from 50 to 3000, with calibration using sodium formate clusters. Samples of 5 µl were introduced by a HP1100 LC system (Hewlett-Packard) connected without column, using 30% acetonitrile in water (0.2% formic acid) with flow rate of 1 ml/min. Ions of *m/z* 683 were isolated (2 Da isolation window) and fragmented using 26.8 eV, with preset parameters for collision-induced-dissociation (100-500Da: 15-25eV, 500-1000Da: 25-30eV) All MS spectra were analyzed using the Bruker DataAnalysis 4.1 software.

Sequence alignment and structural comparison. Protein sequences of previously characterized AA9 LPMOs were retrieved from GenBank using the following accession numbers (*Pc*LPMO9D: BAL43430, *Nc*LPMO9F: CAD70347, *Mt*LPMO9B: AON76800, *Nc*LPMO9A: EAA30263, *Nc*LPMO9C: EAA36362, *Nc*LPMO9D: CAD21296, *Ls*LPMO9A: ALN96977). Sequences were aligned using the Mega 6.06 software (<http://www.megasoftware.net/>). Published LPMO crystal structures were downloaded from the Protein Database Bank (<http://www.rcsb.org/pdb/home/home.do>) with corresponding accession numbers (*Pc*LPMO9D: 4B5Q, *Nc*LPMO9F: 4EIR, *Nc*LPMO9A: 5FOH, *Nc*LPMO9C: 4D7V, *Nc*LPMO9D: 4EIR, *Ls*LPMO9A in complex with a cellotriose ligand: 5ACF). Previously published atomic coordinates of computational simulations of the binding of *Pc*LPMO9D onto crystalline cellulose surface was kindly provided by Dr. Gregg Beckham from National Renewable Energy Laboratory, USA. Structural comparisons and visualization were performed using PyMol molecular graphing software (DeLano Scientific LLC, San Carlos, USA).

Results

Heterologous expression of LPMOs from *H. irregulare* in *P. pastoris*

Two *H. irregulare* LPMOs that had previously showed highly increased transcription levels when the fungus was grown on woody biomass materials, *HiLPMO9H* (GeneBank accession AFO72237) and *HiLPMO9I* (GeneBank accession AFO72238) were successfully expressed in *P. pastoris* after CRISPR/Cas9-mediated gene recombination. The search of conserved domains (<https://www.ncbi.nlm.nih.gov/Structure/cdd/wrpsb.cgi>) revealed that both *HiLPMO9H* and *HiLPMO9I* contain an N-terminal AA9 catalytic domain (translated peptide sequence: 18 to 255 for *HiLPMO9H*, 20–233 for *HiLPMO9I*), a CBM1 domain (*HiLPMO9H*: 309–342, *HiLPMO9I*: 283–315) and a linker region (*HiLPMO9H*: 256–308, *HiLPMO9I*: 234–282) that connects the AA9 catalytic module to the CBM1 domain (Fig 1A). A sequence alignment of the protein sequences of the corresponding modules of these two LPMOs reveal that the sequence similarity of the catalytic domain (45% identical) is lower than the CBM 1 domain (65% identical). *HiLPMO9H* and *HiLPMO9I* were predicted to have 37 and 25 O-linked glycosylation sites respectively, but these two LPMOs are not likely to be N-glycosylated due to the lack of potential N-glycosylation sites. The majority of the O-linked glycosylation sites found on *HiLPMO9H* (62%) and *HiLPMO9I* (64%) were predicted to occur on serine or threonine residues of the linker region. Purified *HiLPMO9H* and *HiLPMO9I* were visible as protein bands of 75 kDa and 55 kDa, respectively, when resolved by SDS-PAGE (Fig 1B). Deglycosylation with α -mannosidase was performed to remove potential O-linked glycosyl moieties from the LPMOs expressed in *P. pastoris*. However, no significant reduction in protein mass was observed. The shapes of the two protein bands were slightly broadened, and the observed sizes were larger than the corresponding theoretical molecular weights for the two proteins, 32.5 kDa and 30.7 kDa, respectively (Fig 1A). This difference might be caused by the presence of multiple types of O-linked glycosylation as the result of heterologous protein expression in *P. pastoris*.

Enzyme activity against cellulose

Native and oxidized cello-oligosaccharides were identified from the reactions of *HiLPMO9H* or *HiLPMO9I* on PASC using 1 mM ascorbic acid as the electron donor by high-performance anion exchange chromatography (HPAEC) with pulsed amperometric detection (PAD) (Fig 2). The products generated by *HiLPMO9H* were detected as an array of native cello-oligosaccharides with degree of polymerization (DP) from 3 to 5 as well as C1-oxidized cello-oligosaccharides (DP2–DP7), as shown in Fig 2A. The C1-oxidized products of *HiLPMO9H* were eluted after the native sugars at retention times ranging from 17.4 min to 23.7 min. Native cello-oligosaccharides (DP3 to DP6) as well as C4-oxidized products were detected when *HiLPMO9I* acted on PASC in the presence of ascorbic acid. C4-oxidized cello-oligosaccharides were detected as elution peaks between 21.9 min and 29.4 min (Fig 2B), and similar results have been shown in previous studies on other LPMOs strictly oxidizing at C4, e.g. *NcLPMO9C* [27] and *MtLPMO9C* [34]. No overlapping peaks were found between the chromatographic regions of C1-oxidized products of *HiLPMO9H* and C4-oxidized products of *HiLPMO9I* (Fig 2), indicating that *HiLPMO9H* is strictly active at the C1 position of β -1,4-glycosidic linkages of PASC whereas *HiLPMO9I* performs the oxidation only at the C4 position.

To further study the formation of oxidized cello-oligosaccharides released from PASC by *HiLPMO9H* and *HiLPMO9I*, the hydrolysates were analyzed by electrospray ionization mass spectrometry (ESI-MS). The different cello-oligosaccharides (non-oxidized and oxidized forms) were detected as an array of positive ion clusters with 1+ charge ranging from DP3 to

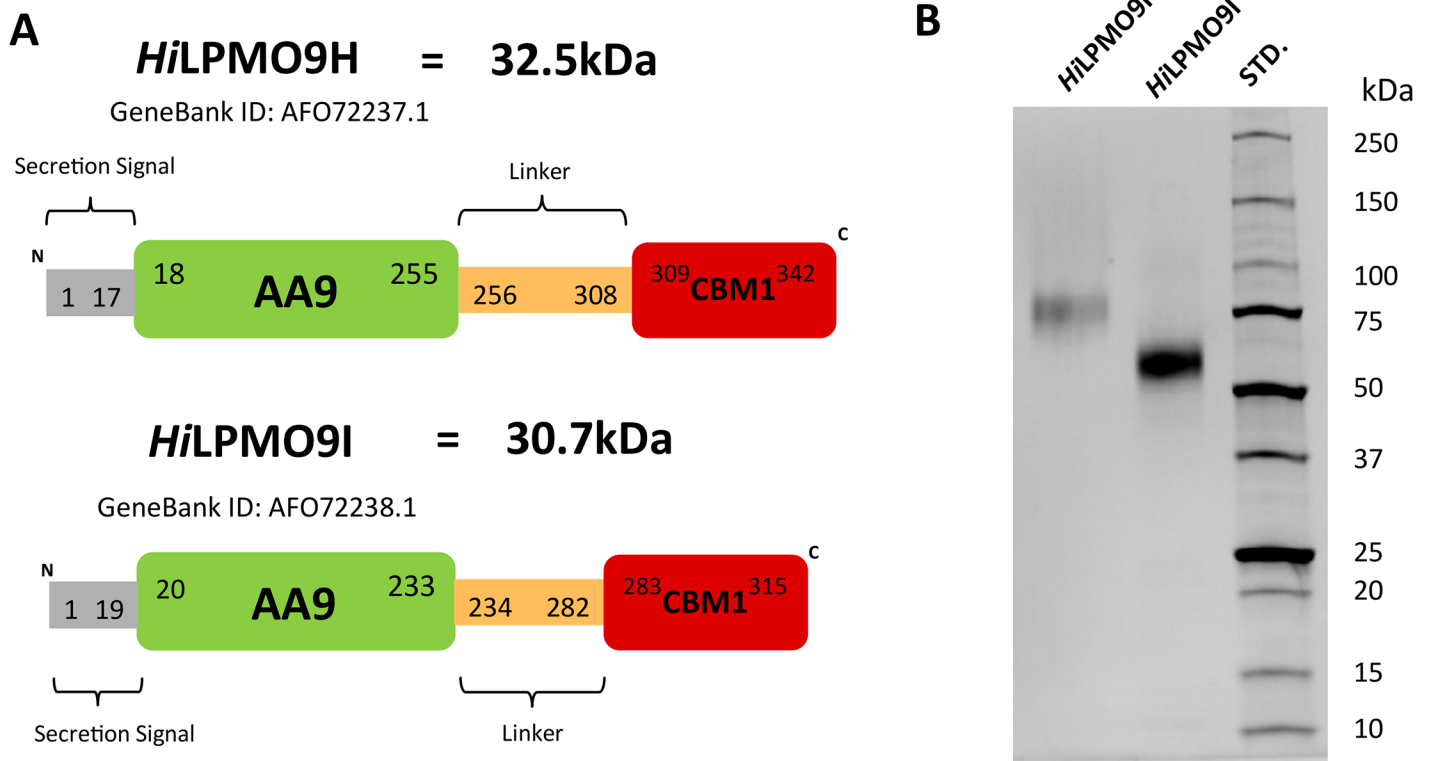


Fig 1. Protein properties of *HiLPMO9H* and *HiLPMO9I* from *H. irregulare*. (A) Schematic illustration of the modular organization of *HiLPMO9H* and *HiLPMO9I*, based on the prediction of conserved domain search using the translated protein sequences. The theoretical molecular weights of the mature protein were calculated while excluding the predicted secretion signal peptides. (B) SDS-PAGE analysis of purified proteins. Lanes from left to right are *HiLPMO9H*, *HiLPMO9I* and protein molecular weight standards (STD).

<https://doi.org/10.1371/journal.pone.0189479.g001>

DP6 (Fig 3). Each cluster contained four types of ions, which correspond to proton adducts of non-oxidized cello-oligosaccharides (mass-to-charge ratios (m/z) = 505, 667, 829, 989; DP3 to DP6), proton adducts of oxidized cello-oligosaccharides (C1-lactone or C4-ketone: m/z 503, 665, 827, 987; C1-aldonic acid or C4-gemdiol: m/z 521, 683, 845, 1005; DP3 to DP6), and sodium adducts of the C1-aldonic acids or C4-gemdiols (m/z +22Da, compared to the corresponding proton adduct). The ions of the highest relative intensity among all the cello-oligosaccharide products in these two reactions were the proton adducts of cellotetraose as C1-aldonic acid (m/z 683.2230 for *HiLPMO9H*) and C4-gemdiol (m/z 683.2258 for *HiLPMO9I*), respectively (Fig 3). These ions were selected for collision-induced fragmentation to further verify the position of oxidization. The MS/MS spectra in both cases showed that the major product ions resulted from breaking glycosidic linkages (Fig 3). For *HiLPMO9H*, fragmentation on the ion with m/z 683.2230 generated two product ions (m/z = 197.0653 and 179.0545) in good agreement with an Y_1 fragment ion of aldonic acid cellotetraose, and its corresponding ion after elimination of water (Y_1-H_2O). Fragmentation of the ion with m/z 683.2258 from the reaction of *HiLPMO9I*, gave two fragment ions (m/z = 143.0341 and 323.0896), which are in line with B_1-2H_2O and Y_2-H_2O , respectively, for a C4-gemdiol cellotetraose.

Enzyme activity against hemicellulose

Samples from the incubation of konjac glucomannan (GM) with LPMOs in the presence of ascorbic acid and samples treated only with an endoglucanase (no ascorbic acid) were analyzed

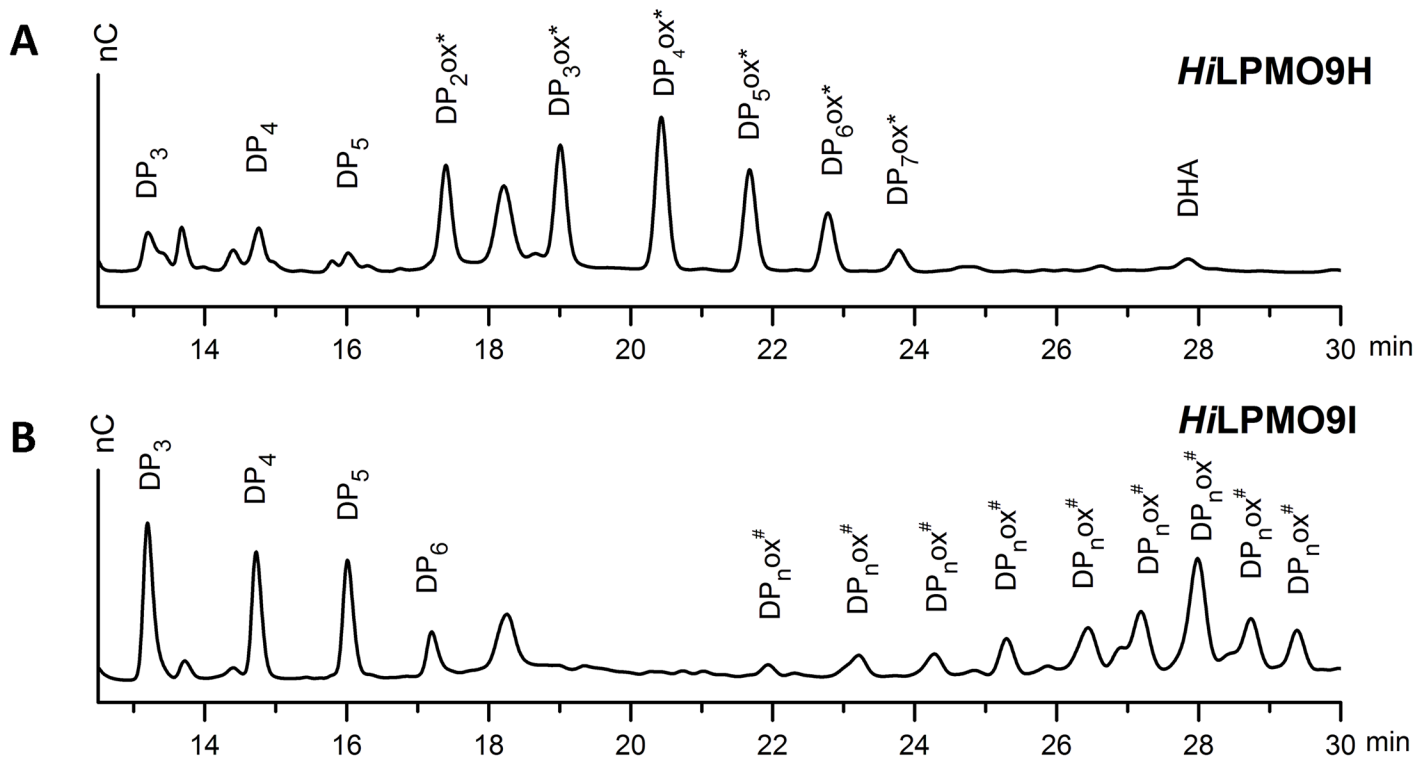


Fig 2. HPAEC-PAD (high performance anion-exchange chromatography with pulsed amperometric detection) analyses of the glucan products after treating PASC with two different *HiLPMOs* using ascorbic acid as the electron donor. (A) HPAEC-PAD elution profile of reaction products of PASC with 1 μ M *HiLPMO9H* in the presence of 1 mM ascorbic acid. DP_n stands for native cello-oligosaccharide. $DP_n ox^*$ represents C1-oxidized aldonic sugars ($DP = 2$ to 6). DHA stands for dehydroascobic acid. (B) HPAEC-PAD elution profile of reaction products when treating PASC with 1 μ M *HiLPMO9I* in the presence of 1mM ascorbic acid. C4-oxidized products are labeled as $DP_n ox^\#$ [27].

<https://doi.org/10.1371/journal.pone.0189479.g002>

using a 75-min gradient HPAEC protocol established by Agger *et al* [28]. The elution pattern of the control reaction (only GM and ascorbic acid) showed a main peak eluted from 40 to 55 min (with the peak center at 49 min), which represented the intact form of the glucomannan polymers in the absence of enzyme. The sample after the treatment with *M. thermophile* endoglucanase 7 (*MtEG7*) (without ascorbic acid added) showed multiple peaks in early stage (9.9 min to 22 min) of the gradient elution and there was no PAD response afterwards, which suggested that the substrate had been degraded into the oligosaccharides with low degree of polymerization. When treating the glucomannan substrate with *HiLPMO9I* in the presence of ascorbic acid, a reduction of polymer size of glucomannan was observed (Fig 4A). The polymer peak center was shifted by 5 min towards an earlier retention time than that of intact polymer in the control sample, and a range of smaller-size oligosaccharides were detected before the main polymer peak (Fig 4A). After further digesting all the reaction products with *MtEG7* and analyzing the products using a shorter HPAEC elution protocol (45 min), a broad range of small peaks (16–34 min retention time) were only observed in the glucomannan sample from the reaction with *HiLPMO9I* after the glucomannan oligosaccharide were eluted (5–14 min; Fig 4B). The additional small peaks were likely oxidized glucomannan oligosaccharides (Fig 4B). When glucomannan was treated with *HiLPMO9H* using ascorbic acid as electron donor, a small shift of the polymer peak center (0.5 min earlier in retention time) was observed and some positive but weak PAD responses were shown in the oligomer regions, compared to the chromatogram of the control, (Fig 4A). However, after further depolymerization using *MtEG7* there was no difference in elution pattern observed between the sample from

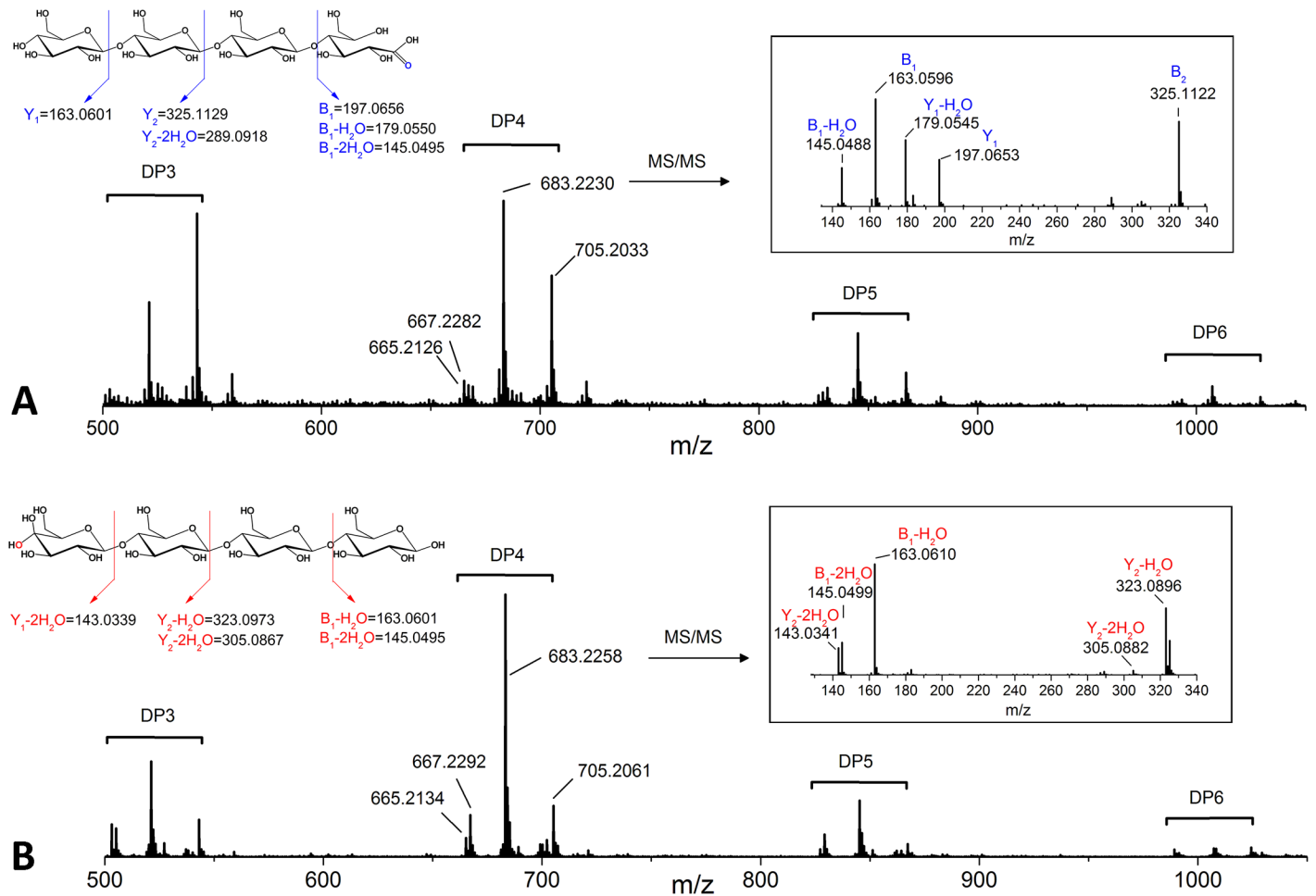


Fig 3. ESI-MS/MS (electrospray ionization tandem mass spectrometry) analyses of the products released by two different *HiLPMOs* when incubated with PASC in the presence of 1mM ascorbic acid. (A) Bottom: mass spectra of cello-oligosaccharides produced by *HiLPMO9H*; Top left: schematic fragmentation pattern of C1-oxidized aldonic cellotetraose and resulting product ions, and both of the precursor ion and fragment ions are proton adducts; Top right: MS/MS spectra of oxidized product with m/z 683.2230. (B) Bottom: mass spectrum of cello-oligosaccharides produced by *HiLPMO9I*; Top Left: schematic fragmentation pattern of C4-oxidized gemdiol cellotetraose and the resulting product ions, and both of the precursor ion and fragment ions are proton adducts; Top right: MS/MS spectra of oxidized product with m/z 683.2258.

<https://doi.org/10.1371/journal.pone.0189479.g003>

HiLPMO9H and the control sample, suggesting that no oxidative cleavage had occurred on the glucomannan substrate during the incubation with *HiLMO9H* in the presence of ascorbic acid (Fig 4B).

Matrix-assisted laser desorption/ionization time-of-flight mass spectrometry (MALDI-TOF MS) confirmed that oxidized products were generated from glucomannan by *HiLPMO9I* using ascorbic acid as electron donor (Fig 5A). MALDI-TOF MS analysis showed that a wide range of native and oxidized oligosaccharides were generated (DP3 to DP13) after treated with *HiLPMO9I*, whereas only native glucomannan oligosaccharides were detected in the sample after incubation with *MtEG7* (DP3 to DP8) (Fig 5A). The difference of the products from the separate treatment of *HiLPMO9I* and *MtEG7* are illustrated by comparing the product profiles at DP6 (Fig 5B). In both cases the main products were sodium adducts of native oligosaccharides, with or without substitution by acetyl groups, which were represented by ions with m/z 1013.3 ($n = 6$), 1055.4 ($n = 6, +1Ac$) 1097.3 ($n = 6, +2Ac$). A small proportion of potassium adducts of corresponding native oligosaccharides (m/z 1029.3 and 1071.4) were also detected.

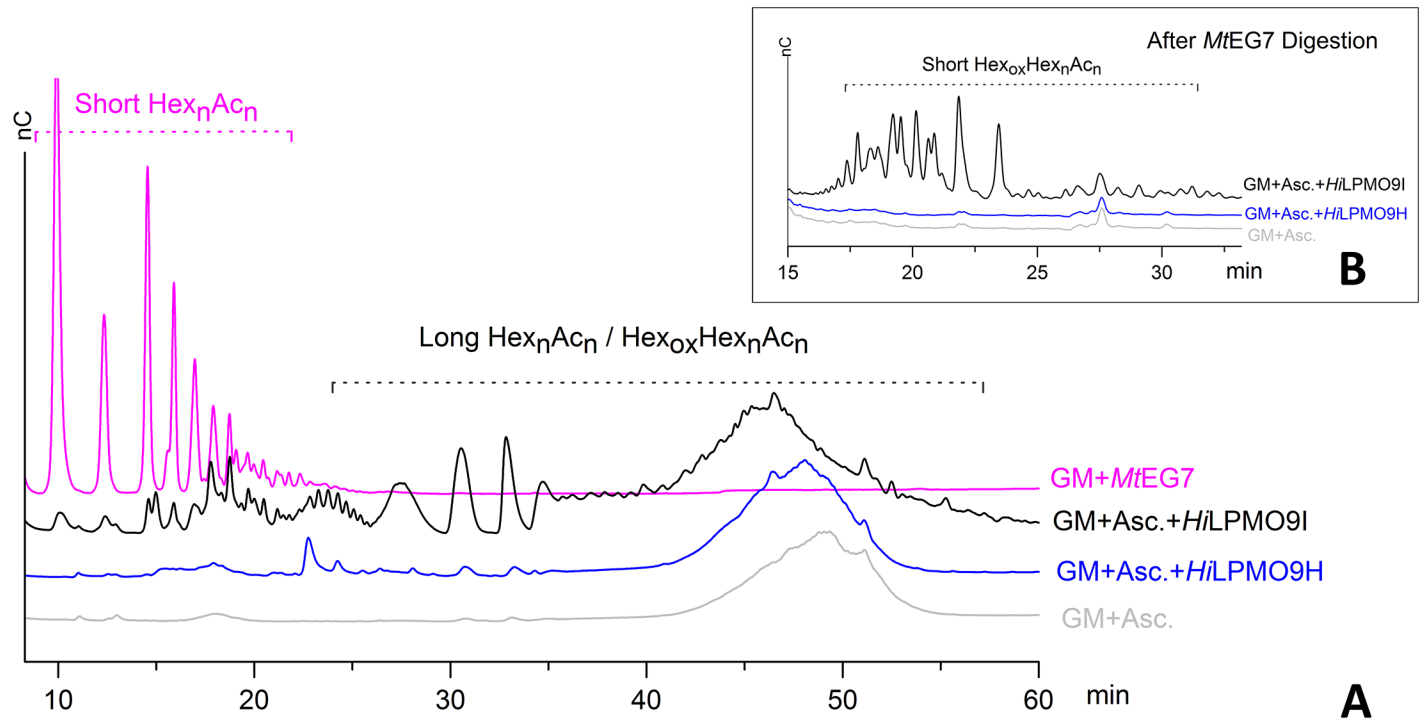


Fig 4. HPAEC-PAD elution profile of glucomannan samples after incubation with different types of enzymes. (A) when incubated with 1mM ascorbic acid alone (light grey), *HiLPMO9H* and 1mM ascorbic acid (blue), *HiLPMO9I* and 1mM ascorbic acid (blue) or *MIEG7* alone (Pink). The abbreviation “Hex” stands for the backbone hexose (glucose or mannose) and “Ac” represents the potential substitution of acetyl groups on C6 of hexose. (B) HPAEC-PAD elution profile of the samples after further depolymerization using *P. pastoris*-expressed *MIEG7*. All the samples were incubated with 1μM *MIEG7* at 37°C for 1 h prior to HPAEC-PAD analysis. The HPAEC-PAD analysis was performed using a shorter elution gradient (45-min for better visualization of peaks representing short oxidized glucomannan residues. The main difference among the elution profiles are mainly found between 15 min to 30 min. Short native glucomannan eluted before 15 min are not shown), in which no difference in elution pattern were found among three individual runs.

<https://doi.org/10.1371/journal.pone.0189479.g004>

Besides native glucomannan oligosaccharides, oxidized oligosaccharides were produced by *HiLPMO9I*, which were present as ions sodium adducts with *m/z* 1011.3, 1053.4 and 1097.3 or potassium adducts with *m/z* 1027.3 and 1069.4.

Regio-selectivity and substrate specificity

HiLPMO9H and *HiLPMO9I*, were incubated separately with a range of cellulosic and hemicellulosic substrates to determine the substrate specificity, and the generation of oxidized product was examined by HPAEC-PAD and mass spectrometric analysis. The results from these studies are summarized in Table 2. *HiLPMO9H* showed oxidative cleaving activity against insoluble cellulose (PASC), but not on soluble cellulose derivative CMC or on short cello-oligosaccharides (G6). For *HiLPMO9H*, no activity was found on the hemicellulosic substrates tested. *HiLPMO9I* was active on PASC, but no activity was observed against other single-chain cellulosic substrates (CMC and G6). *HiLPMO9I* could oxidatively cleave konjac plant glucomannan with heterogeneous backbone composed of glucose and mannose, whereas it could not cleave locus bean gum galactomannan with β-1,4-linked mannose backbone. This suggested that the oxidative cleavage occurred on the β-1,4-glycosidic linkage of glucomannan. No activity against other hemicellulosic substrates was detected for *HiLPMO9I*, including tamarind xyloglucan, barley β-1,3-1,4-glucan and birchwood xylan.

Sequence alignment and structural comparison. The structural overlay (Fig 6A) showed that the major differences on the potential substrate binding surface between C1-specific and

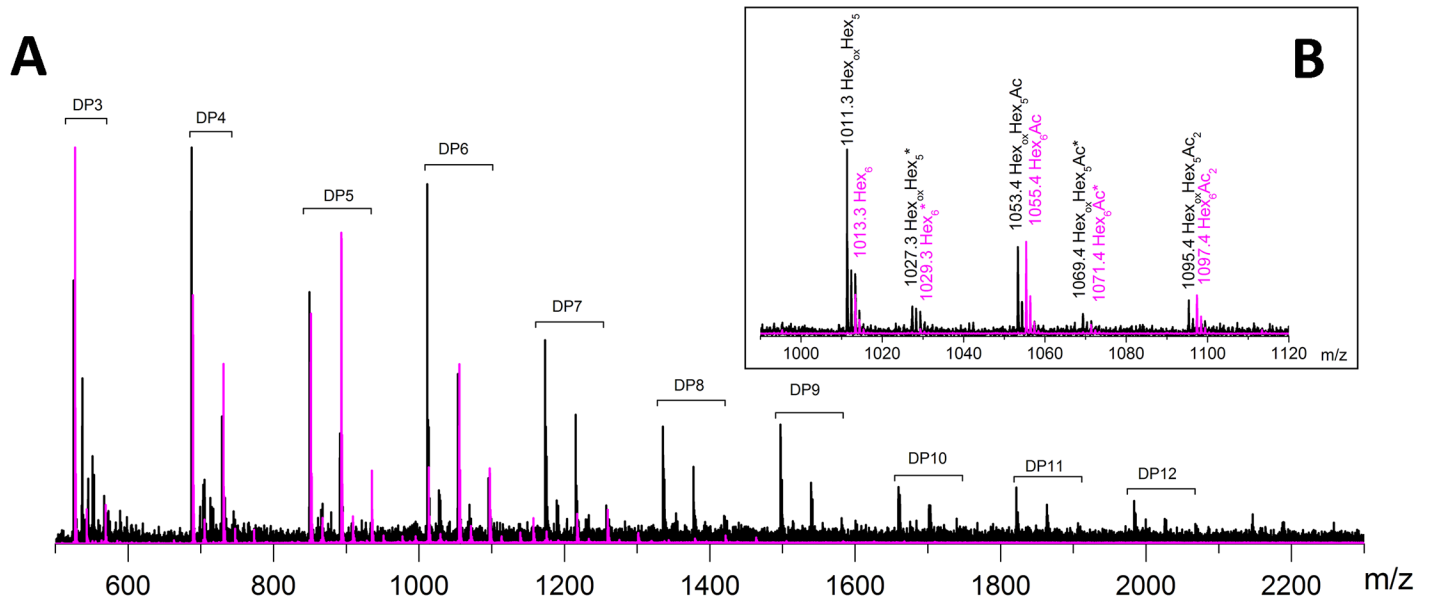


Fig 5. MALDI-TOF MS (matrix assisted laser desorption ionisation time-of-flight mass spectrometry) analysis for comparing the product profiles of *MIEG7* expressed in *P. pastoris* and *HILPMO9I* expressed in *P. pastoris* after incubation with glucomannan. (A) MALDI-TOF MS spectrum of reaction products after incubation with *MIEG7* alone (pink), and with *HILPMO9I* in the presence of ascorbic acid (black). (B) Comparative view of products at DP6 generated by *MIEG7* (pink) or *HILPMO9I* (black). Oxidized glucomannan oligosaccharides were detected in the spectra of *HILPMO9I* (black), represented as ions with 2 Da less than the native products (pink). Ions labeled with start mark (*) are potassium adducts. Ions without special mark are sodium adducts.

<https://doi.org/10.1371/journal.pone.0189479.g005>

C4-specific AA9 LPMOs were observed on the L3 loop (between $\beta 5$ and $\beta 6$), where the second conserved histidine comprising the Cu-binding site is located (Fig 6A). A relatively short L3 loop (around 10 residues) has been observed in the structures of two C1-active LPMOs (*PcLPMO9D* and *NcLPMO9F*) (Fig 6B). In contrast, the L3 loop of two C4-specific LPMO (*NcLPMO9A* and *NcLPMO9C*) are found to be extended to 19 and 23 amino acid residues, respectively (Fig 6B and 6C). A multiple sequence alignment of all known C4-specific LPMOs, including the C4-oxidizing *HiLPMO9I* in our studies, reveal that the first residue of the L3 loop is an aromatic residue (histidine or tyrosine), and the residue right before the second histidine residue coordinating the catalytic copper in the active site is found to be a serine in all included

Table 2. Regio-selectivity and substrate specificity of *HiLPMO9B* and *HiLPMO9I*.

	<i>HiLPMO9B</i>	<i>HiLPMO9I</i>
Regio-selectivity	C1	C4
Cellulosic substrate		
PASC	+	+
CMC	-	-
Cellohexose	-	-
Hemicellulosic substrate		
Xyloglucan	-	-
Glucomanan	-	+
β -1,3-1,4-glucon	-	-
β -Galactomannan	-	-
Glucuronoxylan	-	-

<https://doi.org/10.1371/journal.pone.0189479.t002>

residues before the second active-site histidine residue is instead an aspartic acid or alanine (Fig 6C).

Discussion

The abundance of putative carbohydrate degrading enzymes identified by a genomic sequencing approach reveal that the white rot fungus *H. irregulare* possess an extensive enzymatic machinery for degradation of complex plant polysaccharides [11,23]. Previously published transcriptomic studies suggested that the putative enzymes encoded by genes that were up-regulated when the fungus was grown on woody biomaterials might be employed for the depolymerization of lignocellulosic substrates in natural environment [11,39]. In this study, two of *H. irregulare*'s CBM-containing AA9 proteins (*HiAA9H*, *HiAA9I*) were confirmed to be oxidative cellulolytic enzymes. The CBM1 domain of these two LPMOs have high sequence similarity, and both are predicted to be cellulose binding modules. These two LPMOs were found to have different regio-selectivities when catalyzing oxidative cleavage of insoluble cellulose. *HiLPMO9H* specifically oxidized at the C1 position of the pyranose rings on the β -1,4-glycosidic linkages, whereas *HiLPMO9I* specifically oxidized at the C4 position of the glucose units on the internal bonds.

Despite the abundance of putative AA9-encoding genes in fungal genomes only a few AA9 enzymes have been biochemically characterized to date. In addition to the two AA9 LPMOs characterized in this study, only 26 other AA9 LPMOs have previously been characterized in terms of regio-selectivity and substrate specificity, among the 1803 putative AA9 LPMOs detected in 218 sequenced fungal genomes currently available [44]. The correlation between substrate specificity of LPMO and their potential contribution on plant-polysaccharide degradation possessed by fungi has been discussed in several previous studies [28,32,34]. For C1-specific LPMOs only cellulolytic activity has been reported [18,31,32,34,43], whereas C4-specific LPMOs and LPMOs oxidizing at both the C1 and the C4 position (C1/C4-active LPMO) show broader substrate specificities with activities on hemicellulose and/or soluble cellulosic fractions, in addition to insoluble cellulose [27,28,32,37,45]. Similarly, the C1-specific *HiLPMO9H* characterized in this study only has activity against PASC, among the range of cellulosic and hemicellulosic substrates tested. The C4-specific *HiLPMO9I* has a wider substrate specificity and has activity also against both insoluble cellulose and glucomannan.

Plant cell wall hemicellulose composition varies widely between different plant species, tissue type as well as the developmental stage of the plant. The vast majority of LPMOs with reported hemicellulolytic activities have been shown to be active on xyloglucan, which is the main component of the primary plant cell wall [28,32]. Xyloglucan-active LPMOs either cleave strictly at the β -1,4-glycosidic bonds without xylose substitution [28,32], or randomly cleave the xyloglucan backbone regardless of the side-chain substitution [28,32]. However, the conventional woody biomaterials contain mainly secondary cell walls, in which xylan and glucomannan are the dominant compounds in hemicellulose fractions of both hardwood and softwood [4]. To the date, only a few studies have reported LPMOs that display activity against various xylan or glucomannan structures. Oxidative cleaving activity against xylan has so far only been reported for three LPMOs from *Myceliophthora thermophila* [33,34], and the xylan cleaving activities were only detected when testing these enzymes on glucuronoxylan substrates in complex with amorphous cellulose. Two of the *M. thermophila* LPMOs also show activities against xyloglucan and various mixed-linkage β -glucan [33,34], but no activity against glucomannan has been reported among these enzymes [33,34]. With exception to the present study, only three studies have reported LPMOs that display activity against glucomannan so far [28,37,46]. One such case is the *N. crassa* C4-specific LPMO *NcLPMO9C*, which

cleaves glucomannan and several other hemicellulosic substrates containing β -1,4-glycosidic bonds, including xyloglucan and β -1,3-1,4-linked glucan from barley and lichen [27,28]. *NcLPMO9C* has been shown to only cleave the substrate at the main-chain glycosidic linkages where the glucose units are not decorated with other sugar moieties, when the enzyme was tested on short xyloglucan and β -1,3-1,4-linked glucan oligosaccharides. This suggests that *NcLPMO9C* probably only acts on glycosidic linkages without acetylation of the glucomannan substrates. However, this hypothesis is yet not experimentally verified. The second example is the C1/C4-active *GtLPMO9A-2*, which also shows a relatively weak glucomannan cleaving activity compared to its activity against xyloglucan. This was demonstrated by the ability of this enzyme to reduce the viscosity of the substrate in the presence of dithiothreitol [37]. Compared to *NcLPMO9C*, *GtLPMO9A-2* cleaves at any β -linkage of xyloglucan backbone regardless of the xylose substitution. The authors of the study proposed that *GtLPMO9A-2* most likely is employed for degradation of xyloglucan in the enzymatic system of this brown-rot fungus. A recent study by Simmons and coworkers has shown that *LsLPMO9A* and *CvLPMO9A* are able to oxidatively cleave glucosyl-1,4-mannosyl linkages on the backbone of glucomannan, but these two LPMOs have also been shown to have activities against other hemicellulose polysaccharides [46]. In the present study, it was shown that *HiLPMO9I* only displays activity against glucomannan and not against other β -linked hemicellulosic substrates, and therefore possesses a stricter substrate preference than the other currently known glucomannan-active LPMOs. The strict glucomannan cleaving preference of *HiLPMO9I* suggests that this enzyme is less likely to act only on the non-substituted glycosidic bonds in the manner of *NcLPMO9C*. There might therefore be some important underlying structural features that contribute to its strict specificity against glucomannan. From a biological perspective, this would also suggest that *HiLPMO9I* is an important component in the hemicellulolytic enzyme systems of *H. irregulare*, by specifically cleaving glucomannan by an oxidative mechanism during the fungus decomposition of the hemicellulose fractions of softwood.

Cellulose microfibrils in plant cell walls are covered by a sheath of hemicellulose polysaccharides, such as xylan, glucuronoxylan, arabinoxylan, glucomannan, and xyloglucan. [3]. The hemicellulose polysaccharides that are wrapped over the cellulose microfibrils act as protective barriers against the cellulolytic-specific enzymes by preventing these enzymes from accessing and depolymerizing the cellulose. It is known that fungi also secrete a range of hemicellulases such as β -glucanases, xylanases and mannanases in order to break up the hemicellulose wrapping and thereby increase the accessibility of the substrate for cellulases [47]. A previous study tested the activity of an LPMO against a PASC-hemicellulose complex substrate and it was shown that a LPMO without xyloglucan cleaving activity (*NcLPMO9A* from *N. crassa*) could not generate oxidized cello-oligo products when incubated with PASC due to the protection by xyloglucan. However, oxidative cleavage activity against PASC was detected after the removal of the xyloglucan shield by using a xyloglucanase prior to treating this substrate with the LPMO [45]. The activities of *HiLPMO9I* against both insoluble cellulose and glucomannan suggest that this enzyme could play multiple roles in the degradation process of both the hemicellulose and cellulose fractions of softwood, and thereby increasing the accessibility of the substrate for other cellulose-specific LPMOs, e.g. *HiLPMO9H*. The proposed synergy between different enzyme types could be a part of a well-orchestrated enzyme machinery that increases the utilization efficiency of available carbon sources for the growth of *H. irregulare* on wood.

Much effort has been made to investigate the interactions between LPMOs and their potential substrates in order to understand the structural basis of the regio-selectivity that individual AA9 LPMOs possess, which have been shown biochemically [22,48,49]. The positioning of the intermediate species (Cu(II)-superoxyl or Cu(II)-oxyl) in the active site of the LPMO is thought to have a major impact on the selectivity of the oxidation of the glycan, and the way

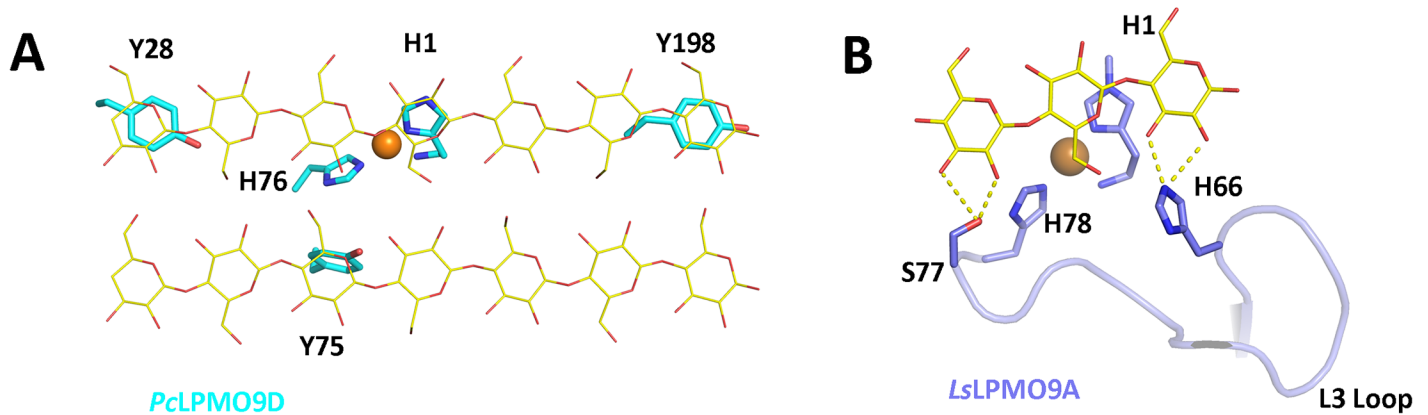


Fig 7. Different types of proposed LPMO-substrate interactions and comparative view on structural features of flat substrate-binding surface of LPMOs. (A) Superposition of the flat surface of C1-specific *PcLPMO9D* structure (PDB ID: 4B5Q) onto a modeled cellulose surface. (B) Protein-ligand interaction of the C4-specific *L. similis* *LsLPMO9A* (expressed in *Aspergillus oryzae*) in complex with cellotriase with the L3 loop indicated (PDB ID: 5ACF).

<https://doi.org/10.1371/journal.pone.0189479.g007>

that LPMO interacts with the substrate is regarded as one of the key determinant factors for the catalytic reaction mechanism of this class of enzymes [48,50]. Recent studies have shown that the C1-specific and C4-specific AA9 LPMOs may interact with cellulose substrate in different ways. Computational simulation studies with a C1-specific LPMO from *Phanerochaete chrysosporium* (*PcLPMO9D*) showed that the characterized LPMO could be absorbed onto a crystalline cellulose surface via hydrophobic interaction by positioning three tyrosine residues (Y28, Y75 and Y198) on the flat protein surface over glucose moieties in the cellulose chains (Fig 7A) [48]. A recent study [49] showed that a C4-specific LPMO from *Lentinus similis* (*LsLPMO9A*) could interact with a cello-oligo ligand (cellotriase (PDB ID: 5CAF) or cellohexose (PDB ID: 5CAI)) via hydrogen-bonding. The residues His66 and Ser77 located on the L3 loop of *L. similis* *LsLPMO9A* were involved in hydrogen bonding interactions with the substrate in both cases (Fig 7B). Interestingly, the L3 loop of AA9 LPMOs is the most variable region on the potential substrate binding surface of these enzymes, with respect to both the length and the conformation when comparing different subclasses of LPMOs (Fig 6B and 6C). Multiple sequence alignment suggests that a long L3 loop region is observed in both C1-specific and C4-specific LPMOs, but C4-specific LPMOs can be distinguished from C1-specific LPMOs if there is an aromatic residue (histidine or tyrosine) as a first residue in the L3 loop region and a serine residue right before the second histidine residue coordinating the catalytic copper in the active site (Fig 6C). The presence of two additional conserved residues on the L3 loop that are specifically observed among C4-specific LPMOs (Fig 6C), and their potential potency of interaction with target substrate via hydrogen bonding (Fig 7B), suggest that there might be some correlation between those features and their strict C4 oxidizing activity.

In summary, this study has characterized two out of the ten putative AA9 LPMOs from *H. irregulare*; *HiLPMO9H* and *HiLPMO9I*, and this is the first biochemical characterization study of the oxidative biomass-degrading enzyme system of this white-rot fungus. These two LPMOs cleave the glycosidic linkages in cellulose by oxidizing different carbon positions of the glycan. The difference in oxidation preference on cellulose between the two LPMOs suggests that this fungus most likely utilize more than one of its set of LPMOs for the degradation of cellulose. Further biochemical studies of *HiLPMO9H* and *HiLPMO9I*, with the focus on comparing the actions of these two enzymes on cellulose surface, could provide more insight regarding the diversity of different types of LPMOs on cellulose degradation. *HiLPMO9H*

only displayed activity against insoluble cellulose, whereas *HiLPMO9I* possessed a broader substrate specificity with activity against both cellulose and glucomannan. The different substrate specificities indicate that these two *H. irregulare* LPMOs might both play important but different roles in plant-cell-wall depolymerization during degradation of softwood biomass by this fungus. The development of methods for precise genome editing in *H. irregulare* would enable gene knock-out experiments to confirm the proposed roles of *HiLPMOs* in lignocellulosic degradation.

Acknowledgments

We thank Madhu Nair Muraleedharan from Luleå University of Technology, Sweden for providing a sample of purified *MtEG7*; and Per Andrén and Anna Nilsson from Uppsala University, Sweden for the access to and assistance with the MALDI-TOF MS instrument.

Author Contributions

Conceptualization: Bing Liu, Åke Olson, Anders Broberg, Mats Sandgren.

Formal analysis: Bing Liu, Åke Olson, Miao Wu, Anders Broberg.

Funding acquisition: Mats Sandgren.

Investigation: Bing Liu, Åke Olson, Anders Broberg.

Methodology: Bing Liu, Anders Broberg.

Project administration: Mats Sandgren.

Resources: Mats Sandgren.

Supervision: Mats Sandgren.

Visualization: Bing Liu, Anders Broberg.

Writing – original draft: Bing Liu, Åke Olson, Miao Wu, Anders Broberg, Mats Sandgren.

Writing – review & editing: Bing Liu, Åke Olson, Miao Wu, Anders Broberg.

References

1. Mäkelä MR, Donofrio N, de Vries RP. Plant biomass degradation by fungi. *Fungal Genet Biol.* 2014; 72: 2–9. <https://doi.org/10.1016/j.fgb.2014.08.010> PMID: 25192611
2. Blanchette RA, Nilsson T, Daniel G, Abad A. Biological Degradation of Wood. *Archaeological Wood.* American Chemical Society; 1989. pp. 141–174.
3. Ochoa-Villarreal M, Aispuro-Hernandez E, Vargas-Arispuro I, Angel M. Plant cell wall polymers: function, structure and biological activity of their derivatives. In: De Souza Gomes A, editor. *Polymerization.* InTech; 2012. <http://www.intechopen.com/books/polymerization/plant-cell-wall-polymers-function-structure-and-biological-activity-of-their-derivatives>
4. Scheller HV, Ulvskov P. Hemicelluloses. *Annu Rev Plant Biol.* 2010; 61: 263–289. <https://doi.org/10.1146/annurev-arplant-042809-112315> PMID: 20192742
5. Woodward S, Stenlid J, Karjalainen R, Hüttermann A. *Heterobasidion annosum*. biology, ecology, impact and control. *CAB Int Camb.* 1998; <http://onlinelibrary.wiley.com/doi/10.1046/j.1365-3059.1999.0366b.x/abstract>
6. Asiegbu FO, Adomas A, Stenlid J. Conifer root and butt rot caused by *Heterobasidion annosum* (Fr.) Bref. s.l. *Mol Plant Pathol.* 2005; 6: 395–409. <https://doi.org/10.1111/j.1364-3703.2005.00295.x> PMID: 20565666
7. Otrosina WJ, Garbelotto M. *Heterobasidion occidentale* sp. nov. and *Heterobasidion irregulare* nom. nov.: a disposition of north american *Heterobasidion* biological species. *Fungal Biol.* 2010; 114: 16–25. <https://doi.org/10.1016/j.mycres.2009.09.001> PMID: 20965057
8. Korhonen K. Intersterility groups of *Heterobasidion annosum*. *Commun Instituti For Fenn.* 1978; 94: 25.

9. Chase TE, Ullrich RC. *Heterobasidion Annosum*, root- and butt-rot of trees. *Adv Plant Pathol.* 1988; 6: 501–510. <https://doi.org/10.1016/B978-0-12-033706-4.50037-2>
10. Capretti P, Korhonen K, Mugnai L, Romagnoli C. An intersterility group of *Heterobasidion annosum* specialized to *Abies alba*. *Eur J For Pathol.* 1990; 20: 231–240. <https://doi.org/10.1111/j.1439-0329.1990.tb01134.x>
11. Olson Å, Aerts A, Asiegbu F, Belbahri L, Bouzid O, Broberg A, et al. Insight into trade-off between wood decay and parasitism from the genome of a fungal forest pathogen. *New Phytol.* 2012; 194: 1001–1013. <https://doi.org/10.1111/j.1469-8137.2012.04128.x> PMID: 22463738
12. Hemsworth GR, Johnston EM, Davies GJ, Walton PH. Lytic polysaccharide monooxygenases in biomass conversion. *Trends Biotechnol.* 2015; 33: 747–761. <https://doi.org/10.1016/j.tibtech.2015.09.006> PMID: 26472212
13. Vaaje-Kolstad G, Westereng B, Horn SJ, Liu Z, Zhai H, Sørle M, et al. An oxidative enzyme boosting the enzymatic conversion of recalcitrant polysaccharides. *Science.* 2010; 330: 219–222. <https://doi.org/10.1126/science.1192231> PMID: 20929773
14. Vaaje-Kolstad G, Bøhle LA, Gåseidnes S, Dalhus B, Bjørås M, Mathiesen G, et al. Characterization of the chitinolytic machinery of *enterococcus faecalis* V583 and high-resolution structure of its oxidative CBM33 enzyme. *J Mol Biol.* 2012; 416: 239–254. <https://doi.org/10.1016/j.jmb.2011.12.033> PMID: 22210154
15. Kim S, Ståhlberg J, Sandgren M, Paton RS, Beckham GT. Quantum mechanical calculations suggest that lytic polysaccharide monooxygenases use a copper-oxygen rebound mechanism. *Proc Natl Acad Sci U S A.* 2014; 111: 149–154. <https://doi.org/10.1073/pnas.1316609111> PMID: 24344312
16. Horn SJ, Vaaje-Kolstad G, Westereng B, Eijsink VG. Novel enzymes for the degradation of cellulose. *Biotechnol Biofuels.* 2012; 5: 45. <https://doi.org/10.1186/1754-6834-5-45> PMID: 22747961
17. Johansen KS. Lytic polysaccharide monooxygenases: the microbial power tool for lignocellulose degradation. *Trends Plant Sci.* 2016; 21: 926–936. <https://doi.org/10.1016/j.tplants.2016.07.012> PMID: 27527668
18. Beeson WT, Phillips CM, Cate JHD, Marletta MA. Oxidative cleavage of cellulose by fungal copper-dependent polysaccharide monooxygenases. *J Am Chem Soc.* 2012; 134: 890–892. <https://doi.org/10.1021/ja210657t> PMID: 22188218
19. Eibinger M, Ganner T, Bubner P, Rošker S, Kracher D, Haltrich D, et al. Cellulose surface degradation by a lytic polysaccharide monooxygenase and its effect on cellulase hydrolytic efficiency. *J Biol Chem.* 2014; 289: 35929–35938. <https://doi.org/10.1074/jbc.M114.602227> PMID: 25361767
20. Leggio LL, Welner D, De Maria L. A structural overview of GH61 proteins—fungal cellulose degrading polysaccharide monooxygenases. *Comput Struct Biotechnol J.* 2012; 2: e201209019. <https://doi.org/10.5936/CSBJ.201209019> PMID: 24688660
21. Busk PK, Lange L. Classification of fungal and bacterial lytic polysaccharide monooxygenases. *BMC Genomics.* 2015; 16: 368. <https://doi.org/10.1186/s12864-015-1601-6> PMID: 25956378
22. Leggio LL, Simmons TJ, Poulsen J-CN, Frandsen KEH, Hemsworth GR, Stringer MA, et al. Structure and boosting activity of a starch-degrading lytic polysaccharide monooxygenase. *Nat Commun.* 2015; 6: 5961. <https://doi.org/10.1038/ncomms6961> PMID: 25608804
23. Rytioja J, Hildén K, Yuzon J, Hatakka A, de Vries RP, Mäkelä MR. Plant-polysaccharide-degrading enzymes from basidiomycetes. *Microbiol Mol Biol Rev MMBR.* 2014; 78: 614–649. <https://doi.org/10.1128/MMBR.00035-14> PMID: 25428937
24. Phillips CM, Beeson WT, Cate JH, Marletta MA. Cellobiose dehydrogenase and a copper-dependent polysaccharide monooxygenase potentiate cellulose degradation by *Neurospora crassa*. *ACS Chem Biol.* 2011; 6: 1399–1406. <https://doi.org/10.1021/cb200351y> PMID: 22004347
25. Sigmund C, Kracher D, Scheiblbrandner S, Zahma K, Felice AKG, Harreither W, et al. Characterization of the Two *Neurospora crassa* Cellobiose Dehydrogenases and Their Connection to Oxidative Cellulose Degradation. *Appl Environ Microbiol.* 2012; 78: 6161–6171. <https://doi.org/10.1128/AEM.01503-12> PMID: 22729546
26. Kittl R, Kracher D, Burgstaller D, Haltrich D, Ludwig R. Production of four *Neurospora crassa* lytic polysaccharide monooxygenases in *Pichia pastoris* monitored by a fluorimetric assay. *Biotechnol Biofuels.* 2012; 5: 79. <https://doi.org/10.1186/1754-6834-5-79> PMID: 23102010
27. Isaksen T, Westereng B, Aachmann FL, Agger JW, Kracher D, Kittl R, et al. A C4-oxidizing lytic polysaccharide monooxygenase cleaving both cellulose and cello-oligosaccharides. *J Biol Chem.* 2014; 289: 2632–2642. <https://doi.org/10.1074/jbc.M113.530196> PMID: 24324265
28. Agger JW, Isaksen T, Várnai A, Vidal-Melgosa S, Willats WGT, Ludwig R, et al. Discovery of LPMO activity on hemicelluloses shows the importance of oxidative processes in plant cell wall degradation.

- Proc Natl Acad Sci U S A. 2014; 111: 6287–6292. <https://doi.org/10.1073/pnas.1323629111> PMID: 24733907
29. Tan T-C, Kracher D, Gandini R, Sygmond C, Kittl R, Haltrich D, et al. Structural basis for cellobiose dehydrogenase action during oxidative cellulose degradation. *Nat Commun.* 2015; 6: 7542. <https://doi.org/10.1038/ncomms8542> PMID: 26151670
 30. Bey M, Zhou S, Poidevin L, Henrissat B, Coutinho PM, Berrin J-G, et al. Comparison of two lytic polysaccharide monooxygenases (GH61) from *Podospora anserina* reveals differences upon cello-oligosaccharides oxidation. *Appl Environ Microbiol.* 2012; AEM.02942-12.
 31. Bey M, Zhou S, Poidevin L, Henrissat B, Coutinho PM, Berrin J-G, et al. Cello-oligosaccharide oxidation reveals differences between two lytic polysaccharide monooxygenases (family GH61) from *Podospora anserina*. *Appl Environ Microbiol.* 2013; 79: 488–496. <https://doi.org/10.1128/AEM.02942-12> PMID: 23124232
 32. Bennati-Granier C, Garajova S, Champion C, Grisel S, Haon M, Zhou S, et al. Substrate specificity and regioselectivity of fungal AA9 lytic polysaccharide monooxygenases secreted by *Podospora anserina*. *Biotechnol Biofuels.* 2015; 8: 90. <https://doi.org/10.1186/s13068-015-0274-3> PMID: 26136828
 33. Frommhagen M, Sforza S, Westphal AH, Visser J, Hinz SWA, Koetsier MJ, et al. Discovery of the combined oxidative cleavage of plant xylan and cellulose by a new fungal polysaccharide monooxygenase. *Biotechnol Biofuels.* 2015; 8: 101. <https://doi.org/10.1186/s13068-015-0284-1> PMID: 26185526
 34. Frommhagen M, Koetsier MJ, Westphal AH, Visser J, Hinz SWA, Vincken J-P, et al. Lytic polysaccharide monooxygenases from *Myceliophthora thermophila* C1 differ in substrate preference and reducing agent specificity. *Biotechnol Biofuels.* 2016; 9: 186. <https://doi.org/10.1186/s13068-016-0594-y> PMID: 27588039
 35. Span EA, Suess DLM, Deller MC, Britt RD, Marletta MA. The Role of the Secondary Coordination Sphere in a Fungal Polysaccharide Monooxygenase. *ACS Chem Biol.* 2017; 12: 1095–1103. <https://doi.org/10.1021/acscchembio.7b00016> PMID: 28257189
 36. Patel I, Kracher D, Ma S, Garajova S, Haon M, Faulds CB, et al. Salt-responsive lytic polysaccharide monooxygenases from the mangrove fungus *Pestalotiopsis* sp. NCi6. *Biotechnol Biofuels.* 2016; 9: 108. <https://doi.org/10.1186/s13068-016-0520-3> PMID: 27213015
 37. Kojima Y, Várnai A, Ishida T, Sunagawa N, Petrovic DM, Igarashi K, et al. A Lytic Polysaccharide Monooxygenase with Broad Xyloglucan Specificity from the Brown-Rot Fungus *Gloeophyllum trabeum* and Its Action on Cellulose-Xyloglucan Complexes. *Appl Environ Microbiol.* 2016; 82: 6557–6572. <https://doi.org/10.1128/AEM.01768-16> PMID: 27590806
 38. Jung S, Song Y, Kim HM, Bae H-J. Enhanced lignocellulosic biomass hydrolysis by oxidative lytic polysaccharide monooxygenases (LPMOs) GH61 from *Gloeophyllum trabeum*. *Enzyme Microb Technol.* 2015; 77: 38–45. <https://doi.org/10.1016/j.enzmictec.2015.05.006> PMID: 26138398
 39. Yakovlev I, Vaaje-Kolstad G, Hietala AM, Stefańczyk E, Solheim H, Fossdal CG. Substrate-specific transcription of the enigmatic GH61 family of the pathogenic white-rot fungus *Heterobasidion irregulare* during growth on lignocellulose. *Appl Microbiol Biotechnol.* 2012; 95: 979–990. <https://doi.org/10.1007/s00253-012-4206-x> PMID: 22718248
 40. Guillén D, Sánchez S, Rodríguez-Sanoja R. Carbohydrate-binding domains: multiplicity of biological roles. *Appl Microbiol Biotechnol.* 2010; 85: 1241–1249. <https://doi.org/10.1007/s00253-009-2331-y> PMID: 19908036
 41. Weninger A, Hatzl A-M, Schmid C, Vogl T, Glieder A. Combinatorial optimization of CRISPR/Cas9 expression enables precision genome engineering in the methylotrophic yeast *Pichia pastoris*. *J Biotechnol.* 2016; 235: 139–149. <https://doi.org/10.1016/j.jbiotec.2016.03.027> PMID: 27015975
 42. Wood TM. Preparation of crystalline, amorphous, and dyed cellulase substrates. *Methods Enzymol.* 1988; 160: 19–25. [https://doi.org/10.1016/0076-6879\(88\)60103-0](https://doi.org/10.1016/0076-6879(88)60103-0)
 43. Westereng B, Ishida T, Vaaje-Kolstad G, Wu M, Eijsink VGH, Igarashi K, et al. The Putative Endoglucanase PcGH61D from *Phanerochaete chrysosporium* is a metal-dependent oxidative enzyme that cleaves cellulose. *PLOS ONE.* 2011; 6: e27807. <https://doi.org/10.1371/journal.pone.0027807> PMID: 22132148
 44. Berlemont R. Distribution and diversity of enzymes for polysaccharide degradation in fungi. *Sci Rep.* 2017; 7: 222. <https://doi.org/10.1038/s41598-017-00258-w> PMID: 28302998
 45. Nekiunaite L, Petrović DM, Westereng B, Vaaje-Kolstad G, Hachem MA, Várnai A, et al. FgLPMO9A from *Fusarium graminearum* cleaves xyloglucan independently of the backbone substitution pattern. *FEBS Lett.* 2016; 590: 3346–3356. <https://doi.org/10.1002/1873-3468.12385> PMID: 27587308
 46. Simmons TJ, Frandsen KEH, Ciano L, Tryfona T, Lenfant N, Poulsen JC, et al. Structural and electronic determinants of lytic polysaccharide monooxygenase reactivity on polysaccharide substrates. *Nat Commun.* 2017; 8. <https://doi.org/10.1038/s41467-017-01247-3> PMID: 29057953

47. van den Brink J, de Vries RP. Fungal enzyme sets for plant polysaccharide degradation. *Appl Microbiol Biotechnol.* 2011; 91: 1477–1492. <https://doi.org/10.1007/s00253-011-3473-2> PMID: 21785931
48. Wu M, Beckham GT, Larsson AM, Ishida T, Kim S, Payne CM, et al. Crystal structure and computational characterization of the lytic polysaccharide monooxygenase GH61D from the Basidiomycota fungus *Phanerochaete chrysosporium*. *J Biol Chem.* 2013; 288: 12828–12839. <https://doi.org/10.1074/jbc.M113.459396> PMID: 23525113
49. Frandsen KEH, Simmons TJ, Dupree P, Poulsen J-CN, Hemsworth GR, Ciano L, et al. The molecular basis of polysaccharide cleavage by lytic polysaccharide monooxygenases. *Nat Chem Biol.* 2016; 12: 298–303. <https://doi.org/10.1038/nchembio.2029> PMID: 26928935
50. O'Dell WB, Agarwal PK, Meilleur F. Oxygen Activation at the Active Site of a Fungal Lytic Polysaccharide Monooxygenase. *Angew Chem Int Ed.* 2017; 56: 767–770. <https://doi.org/10.1002/anie.201610502> PMID: 28004877